Feedback active control using an acoustic black hole

K. Hook, S. Daley, J. Cheer
Institute of Sound and Vibration Research, University of Southampton,
Highfield, Southampton, SO17 1BJ, United Kingdom

Abstract
Acoustic black holes (ABHs) are tapered structural features that can achieve high levels of structural damping within lightweight constraints. It has previously been proposed to integrate feedforward active vibration control into an ABH to enable control over a broad spectrum, however, the time advance information required in this control strategy is not always available. Therefore, this paper investigates a feedback control system, where a piezoelectric patch is used to provide the control actuation and a remote damping method is used to examine the different compensators available to control either the local taper vibration or the reflected wave component. The investigation highlights that at most frequencies minimising the taper vibration does not significantly affect the reflected wave, however minimising the reflected wave enhances the taper vibration. It is also shown that in some cases both quantities can be reduced and that it is possible to maintain the passive ABH performance whilst simultaneously limiting the taper vibration, which reduces structural fatigue.

1 Introduction

An ABH can be realised as a smoothly varying structural feature that tapers from a thicker to a thinner profile [1]. The flexural wave speed in a beam can be related to the thickness of the structure and so as a flexural wave travels down the taper its speed is reduced, resulting in a low amount of reflected energy from the tip. In practice, a small amount of damping material is required to achieve good passive performance [2] and it has been shown that this damping material can be optimally placed to minimise vibration [3–5] or radiated sound [6]. The properties of the damping material can also be modified using temperature [7]. In addition to studies into the damping, there have been a variety of studies that examine different ways to tune the narrow and broadband performance of an ABH by varying the geometric design parameters, such as taper length, power law and tip height [3, 4, 8–14]. Different ABH constructions have also been examined such as rolling up a long taper to reduce the size of the ABH whilst maintaining good low frequency performance [15]. In addition to the passive tuning methods available, it has been proposed that active components could be used to enhance an ABH. The active ABH (AABH) could then be subjected to a number of different active control strategies in order to minimise different cost functions and this was demonstrated in the context of a feedforward wave-based control system in [16]. This feedforward control strategy required time-advance knowledge of the disturbance signal, something that is not always available in industrial applications. A feedback approach may, therefore, provide a number of practical benefits and a controller can be designed that uses a local feedback loop to minimise a remote quantity [17–19]. To provide further insight into the effect of wave control and to demonstrate a different approach to using an AABH, this paper presents an investigation into the frequency domain implementation of the feedback remote damping vibration controller designed in [17]. The tradeoff between minimising the local taper vibration and minimising the reflected wave component is examined over a broad frequency range. The paper is organised as follows. Section 2 presents the experimental setup used in this investigation, a brief overview of the wave decomposition method used to estimate the wave components in the structure and uses the geometric controller design from [17] to highlight four control strategies that can be used to calculate a control compensator. Section 3 contains the results from a frequency domain implementation of each control strategy and the conclusions of this work are presented in Section 4.

2 Controller Design

In this section, the geometric controller in [17] is presented for use on an active ABH termination. Initially, the experimental setup is described from which the frequency responses have been acquired. The wave decomposition method used to estimate the reflected wave component is outlined and the frequency responses are then used to examine the tradeoff between minimising the local taper vibration and minimising the reflected wave component. Four control case studies are then selected and the corresponding compensator values are calculated.

2.1 Experimental Setup

Table 1 lists the dimensions of the experimental setup and a diagram of the setup is presented in Figure 1. The primary force, F_P, was implemented by driving a shaker with broadband white noise using a sampling frequency of 22 kHz. The secondary force, F_G, was produced by driving the piezoelectric transducer with broadband white noise using a sampling frequency of 22 kHz. Accelerometers 1 and 2 were used to calculate the reflected wave component in the beam, ϕ^-, and accelerometer 3 was used to measure the local vibration in the taper. The frequency responses measured at each of the locations can be written in terms of contributions

Table 1: Dimensions of the experimental setup

Parameter	Value
Beam length	300 mm
Beam height	10 mm
Beam width	40 mm
ABH length	70 mm
ABH power law	4
ABH tip height	0.5 mm
Piezo length	61 mm
Piezo height	0.4 mm
Piezo width	35 mm

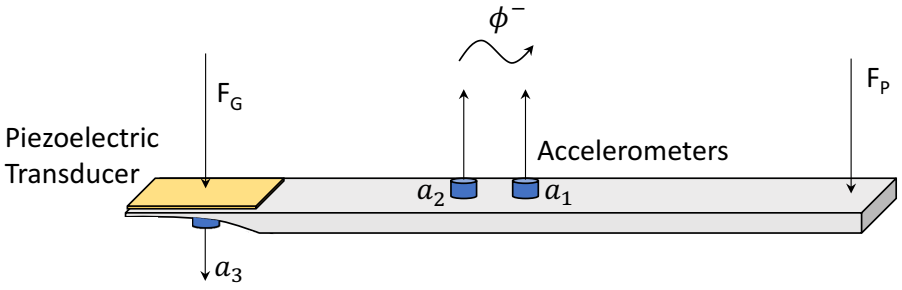

Figure 1: The physical system showing how the local vibration is measured in the taper and the reflected wave is calculated in the beam section.

from the primary and secondary sources as

$$\begin{Bmatrix} \phi^-(\omega) \\ a_3(\omega) \end{Bmatrix} = \begin{bmatrix} g_{11}(\omega) & g_{12}(\omega) \\ g_{21}(\omega) & g_{22}(\omega) \end{bmatrix} \begin{Bmatrix} u(\omega) \\ d(\omega) \end{Bmatrix}, \tag{1}$$

where g_{11} is the frequency response between the piezoelectric transducer and the accelerometer on the taper, g_{12} is the frequency response between the primary force and the accelerometer on the taper, g_{21} is the frequency response between the piezoelectric transducer and the reflected wave component and g_{22} is the

frequency response between the primary force and the reflected wave component [17]. d is the signal driving the primary shaker and the control signal, u, that is used to drive the piezoelectric transducer can be calculated using the feedback control law,

$$u(\omega) = -\kappa(\omega)a_3(\omega). \tag{2}$$

A block diagram of the control system is shown in Figure 2.

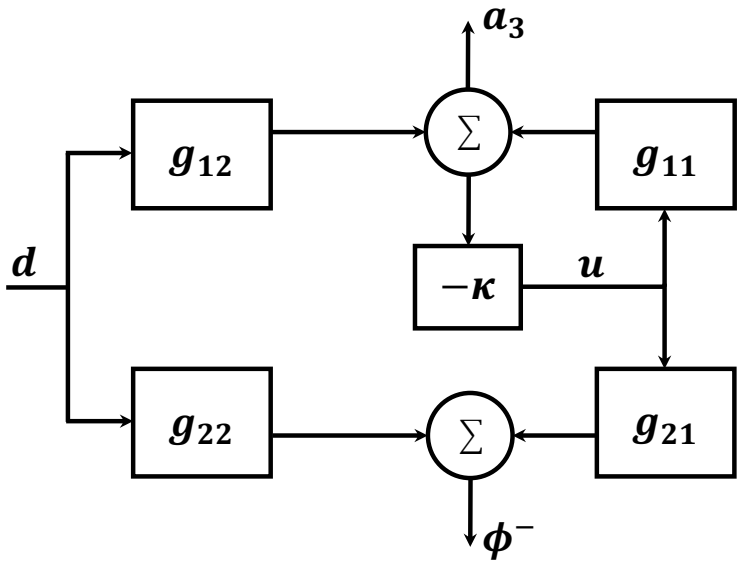

Figure 2: A block diagram showing the feedback control system. The local signal from accelerometer 3 is fed back through a compensator, κ, to obtain the control signal, u. The control signal is used to drive the piezoelectric transducer and the control of both the taper vibration and the reflected wave component can be examined.

2.2 Calculating the reflected wave component

In the frequency domain, the incident and reflected wave components, $\phi^+(\omega)$ and $\phi^-(\omega)$, can be written in terms of the signal measured at the two accelerometers, a_1 and a_2, as

$$\begin{Bmatrix} a_1(\omega) \\ a_2(\omega) \end{Bmatrix} = -\omega^2 \begin{bmatrix} e^{ik\Delta/2} & e^{-ik\Delta/2} \\ e^{-ik\Delta/2} & e^{ik\Delta/2} \end{bmatrix} \begin{Bmatrix} \phi^+(\omega) \\ \phi^-(\omega) \end{Bmatrix}, \tag{3}$$

where ω is the angular frequency, k is the flexural wavenumber and Δ is the sensor separation [20, 21]. Equation 3 can be rearranged to give

$$\begin{Bmatrix} \phi^+(\omega) \\ \phi^-(\omega) \end{Bmatrix} = \begin{bmatrix} (h_1(\omega) - h_2(\omega)) & (h_1(\omega) + h_2(\omega)) \\ (h_1(\omega) + h_2(\omega)) & (h_1(\omega) - h_2(\omega)) \end{bmatrix} \begin{Bmatrix} a_1(\omega) \\ a_2(\omega) \end{Bmatrix}, \tag{4}$$

where

$$h_1(\omega) = \frac{-i}{4\omega\cos(k\Delta/2)}; \qquad h_2(\omega) = \frac{1}{4\omega\sin(k\Delta/2)}. \tag{5}$$

In order to implement Equation 4 in the time domain, $h_1(\omega) + h_2(\omega)$ and $h_1(\omega) - h_2(\omega)$ can be approximated using discrete-time FIR filters [20, 22, 23], which gives the vectors of filter coefficients $\boldsymbol{h}_{1+2}$ and $\boldsymbol{h}_{1-2}$ respectively. To ensure that the filters are causal, a small delay can be applied to the frequency responses prior to calculating the filters. Although effective, these wave decomposition filters are subjected to some limitations imposed by the sensor separation and sensor array location, which results in lower and upper frequency

limits. In this investigation, the frequency range of interest has been limited to 400 Hz – 10 kHz and further information regarding the derivation of these limits can be found in [20, 22, 23].

2.3 Remote Damping Circles

In order to find a compensator, κ, that minimises either or both the local vibration and reflected wave component, the closed loop transfer functions can be written as

$$\left|\frac{1}{1 + g_{11}(\omega)\kappa(\omega)}\right| < 1 \tag{6}$$

$$\left|1 - \frac{\kappa(\omega)g_{12}(\omega)g_{21}(\omega)}{g_{22}(\omega)(1 + g_{11}(\omega)\kappa(\omega))}\right| < 1, \tag{7}$$

where satisfying Equation 6 results in a reduction of the local vibration at accelerometer 3 and satisfying Equation 7 results in a reduction of the reflected wave component [17]. The frequency dependency is suppressed from this point forward for clarity, but it should be assumed unless stated otherwise. As shown in [17], Equation 7 can be also be expressed as

$$|\beta + 1| < 1, \tag{8}$$

where

$$\beta = \left(\frac{1}{1 + g_{11}\kappa} - 1\right)\frac{g_{12}g_{21}}{g_{11}g_{22}} \tag{9}$$

and Equation 6 can be expressed in terms of β as

$$\left|\beta\frac{g_{11}g_{22}}{g_{12}g_{21}} + 1\right| = |\gamma + 1| < 1. \tag{10}$$

Both Equation 8 and Equation 10 describe a unit circle with a centre point (-1, 0) on the complex plane and are expressed in terms of β. Therefore, if Equation 10 is plotted as a unit circle on the complex γ-plane, Equation 8 can be mapped onto the γ-plane as a circle with a centre point at $-\tilde{g}$ [17], where

$$\tilde{g} = \frac{g_{11}g_{22}}{g_{12}g_{21}} \tag{11}$$

and radius $|\tilde{g}|$. The centre point of each of these circles can be used to calculate a compensator that minimises the respective error signal and the points around the outer edge of each circle can be used to calculate a compensator that neither attenuates or enhances the error. Both circles will intersect at the origin (0,0) of the complex plane, which represents no control being implemented. A point, γ, from the complex plane can be selected and the corresponding compensator calculated as

$$\kappa = \frac{\gamma}{(1 + \gamma)g_{11}}. \tag{12}$$

Two examples are given in Figure 3 at 600 Hz and at 5186 Hz. From the results shown in Figure 4(a), it can be seen that the (−1,0) point that corresponds to minimisation of the local vibration lies within the circle of control of the reflected wave. Since the point lies approximately half way between the ± 0 dB circle and the − 6 dB circle, a compensator calculated from this point will result in the reflected wave being attenuated by approximately 3 dB. In this case, a blue circle marks this point because it corresponds to the optimum local vibration reduction without an enhancement of the reflected wave. If, however, the reflected wave is minimised by calculating a compensator from the point $-\tilde{g}$, then the local vibration will be enhanced by a little over 6 dB because this point falls just outside of the + 6 dB circle. To reduce the reflected wave without enhancing the local vibration, the point marked by the blue circle at approximately (−1.9,−0.4) can be used to calculate a compensator. Figure 4(b) shows a similar set of results, however, in this case the frequency being controlled is 5186 Hz. This frequency also represents a more common set of circles, where minimising either quantity will result in enhancement of the other. From these results, it can be seen that

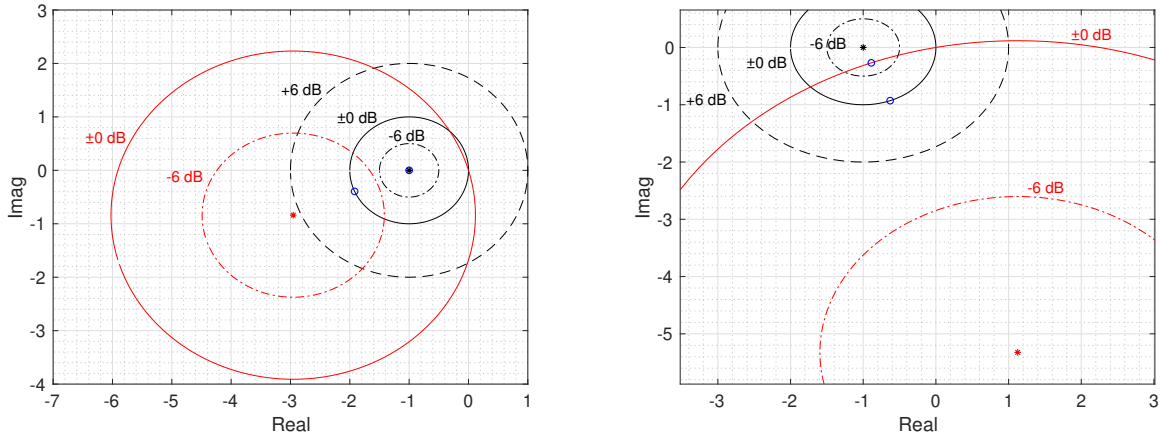

(a) 600 Hz (b) 5186 Hz

Figure 3: The red circle representing control of the reflected wave component plotted with respect to the black unit circle representing control of the local vibration at (a) 600 Hz and (b) 5186 Hz. The solid lines represent 0 dB of attenuation, the dot-dash lines represent 6 dB of attenuation and the asterisk represents minimisation of the respective quantity. The blue circles represent the best possible control in each case without enhancing either the local vibration or the reflected wave component.

a compensator calculated from the $(-1,0)$ point will minimise the local vibration, but will slightly enhance the reflected wave. A compensator calculated from the $-\tilde{g}$ point will minimise the reflected wave but will strongly enhance the local vibration. Calculating a compensator from the blue circle at $(-0.9,-0.3)$ will result in the best possible reduction in the local vibration, approximately 11 dB, without enhancing the reflected wave. Similarly, calculating a compensator from the blue circle at $(-0.6,-0.6)$ will attenuate the reflected wave by approximately 2 dB without enhancing the local vibration. Each of these control cases will be examined in the following section. It is important to note that this implementation has been performed in the frequency domain and does not take into account issues such as stability, robustness and causality that will be present in real-time implementation. Approaches that resolve these issues for the design of a remote vibration controller can be found in [17–19].

3 Frequency Domain Tonal Control

In this section, the results from an offline frequency domain implementation of the 4 control cases highlighted in Section 2.3 are presented. The four control cases are minimisation of the local vibration, minimisation of the reflected wave, reduction of the local vibration without enhancing the reflected wave and reduction of the reflected wave without enhancing the local vibration. In each case, regularisation has been added to the selected γ to constrain the maximum attenuation to approximately 20 dB for clarity and to avoid unrealistic levels of control. The results from these control implementations are presented over a frequency range of 400 Hz – 10 kHz and can be seen in Figure 4.

From the results presented in Figure 4, it can be seen that when control is set to minimise the local taper vibration (shown by the solid blue lines), the vibration in the taper is reduced by approximately 20 dB at all frequencies, which is simply limited by the level of regularisation used in the study. The corresponding reflected wave component is generally unchanged, varying by approximately ± 1 dB over the bandwidth presented. However, there are specific frequencies and frequency bands that are attenuated or enhanced slightly more. For instance, at 600 Hz, the resonant frequency used as an example in Figure 4(a), there is approximately 3 dB of attenuation, which is consistent with the prediction. The band of frequencies around the resonance at 1640 Hz are enhanced by up to 8 dB. The final notable change is the large reduction around 4100 Hz, which is approximately 10 dB.

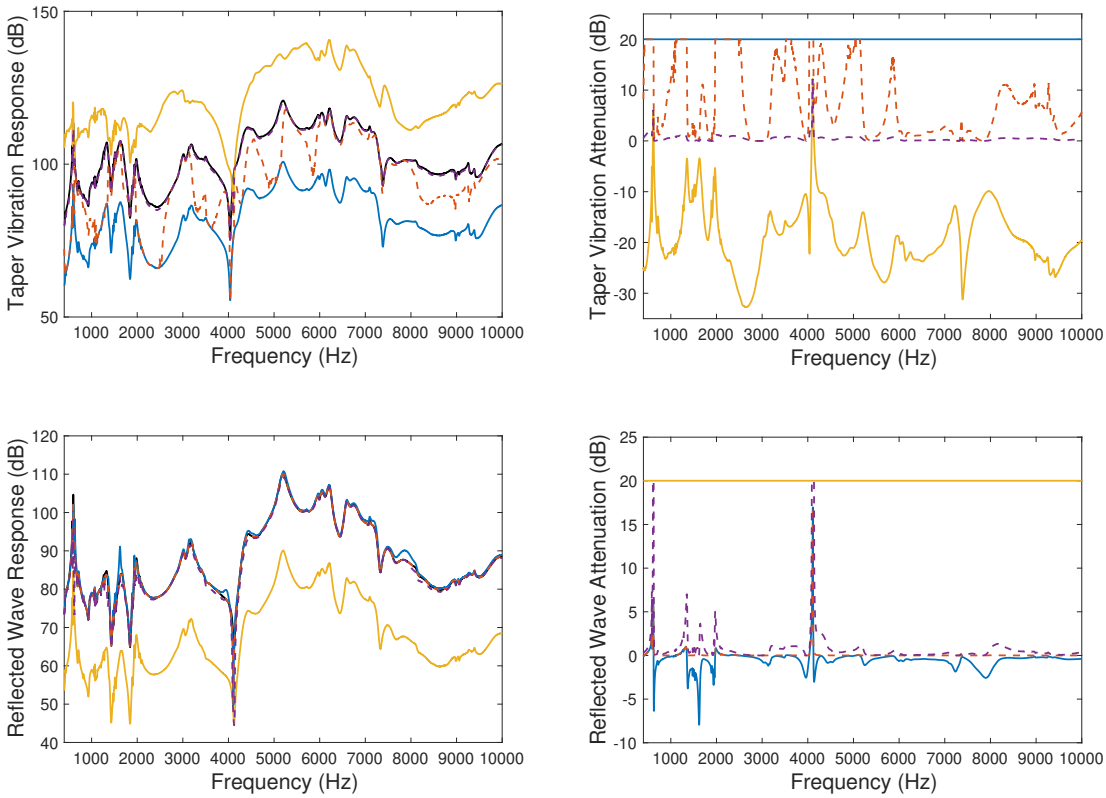

Figure 4: Feedback control implemented for the four cases and presented in terms of the response and attenuation. The effect that each compensator has in the local vibration is shown in the top plots and the effect that each compensator has in the reflected wave is shown in the bottom plots. The uncontrolled case is represented by 0 dB of attenuation, the local minimisation case is represented by a solid blue line, the reflected wave minimisation case is represented by a solid yellow line, the local reduction without enhancement of the reflected wave case is represented by a dashed red line and the reflected wave reduction without enhancement of the local vibration is represented by a purple dashed line.

When control is set to minimise the reflected wave component (shown by the solid yellow lines), the results in Figure 4 show that the reflected wave component is reduced by approximately 20 dB at all frequencies, which is again limited by the selected level of regularisation. It can be seen from the response in the taper, that this control strategy leads to a significant increase in the taper vibration of up to 40 dB. There are, however, two narrow frequency bands where the local vibration is reduced by up to 12 dB and these are around 620 Hz and 4108 Hz. This control strategy is of particular interest because one of the key performance criteria of an ABH is its reflection coefficient. It has been previously shown that the reflection coefficient can be controlled using a feedforward architecture [16] and this study provides more insight into the effect that minimising the reflection coefficient has on the vibration level in the taper. It is clear that vibration is significantly enhanced and this may lead to structural fatigue.

In order to reduce effects of structural fatigue, the reflected wave can be controlled without enhancing the level of vibration in the tip or, alternatively, the local vibration in the tip can be reduced without enhancing the reflected wave component, thus maintaining the passive performance of the ABH whilst reducing structural fatigue. The performance of the former control strategy is shown by the dashed purple line in Figure 4 and the latter control strategy is shown by the dashed red line. When control is implemented to reduce the reflected wave component without enhancing the local vibration in the taper, it can be seen from the results in Figure 4 that there are only two narrow bandwidths where the reflected wave can be reduced by approximately

20 dB without enhancing the taper vibration. These narrow bandwidths occur around 610 Hz – 624 Hz and 4090 Hz – 4134 Hz. There is also a reasonable reduction in the reflected wave of around 6 dB – 8 dB at and around the 200 Hz, 600 Hz, 1328 Hz, 1654 Hz and 1964 Hz resonances. When control is set to reduce the local taper vibration without enhancing the reflected wave component, it can be seen from Figure 4 that there are a number of wide frequency bands where the taper vibration can be reduced by approximately 20 dB without enhancing the reflected wave. These frequency bands are 422 Hz – 622 Hz, 1100 Hz – 1350 Hz, 1970 Hz – 2550 Hz, 3524 Hz – 3620 Hz, 4032 Hz – 4122 Hz and 5044 Hz – 5144 Hz. It can also be seen from the results in Figure 4 that there is a good reduction in the local taper vibration outside of these bands of up to 16 dB.

4 Conclusions

This paper has presented an investigation into the use of feedback control in an active ABH. In this study, a remote damping method has been used to examine how four different control strategies affect the local vibration in the taper and the reflected wave component. The results from this investigation have shown that when the local taper vibration is controlled, there is very little effect on the reflected wave component, which limits the use of this control strategy in the improvement of ABH performance. This indicates that a control strategy such as pure velocity feedback is unlikely to have any significant performance benefits, except perhaps at one or two very specific frequencies. When the reflected wave is controlled, the vibration in the taper is greatly enhanced. This control strategy can be compared to the feedforward control strategy presented in [16] and provides more insight into what actively reducing the reflection coefficient does to the ABH taper. Although the performance has been greatly improved in terms of the reflected wave control, the enhancement of vibration in the thin region of the taper may increase structural fatigue and lead to early failure in industrial applications. When the reflected wave is controlled without enhancing the local vibration in the taper, it has been shown that there are only a small number of narrow bands where a large reduction in the reflected wave can be achieved. However, a reasonable level of control can be performed at the resonant frequencies and so this control strategy may be of interest if examining the radiated sound from the structure, which has not been addressed in this paper. When the local vibration in the taper is controlled without enhancing the reflected wave component, is has been shown that at a significant number of frequencies, including the resonances, the local taper vibration can be greatly reduced without incurring any enhancement in the reflected wave. This control strategy may, therefore, be useful in industrial applications where a passive ABH provides enough damping but is suffering from fatigue due to high vibrational levels in the taper. Therefore, the final two control strategies have shown that, in applications where it may not be suitable to completely minimise the reflected wave in the taper, a compromise can be met where limitations can be set on the vibration level in the taper and the reflection attenuating performance can be maintained or improved whilst adhering to these limits.

Acknowledgements

This work was supported by an EPSRC iCASE studentship (Voucher number 16000058) and an EPSRC Prosperity Partnership (EP/S03661X/1).

References

[1] M. Mironov, "Propagation of a flexural wave in a plate whose thickness decreases smoothly to zero in a finite interval," *Soviet Physics: Acoustics*, vol. 34, no. 3, pp. 318–319, 1988.

[2] V.V. Krylov and F. Tilman, "Acoustic 'black holes' for flexural waves as effective vibration dampers," *Journal of Sound and Vibration*, vol. 274, pp. 605–619, 2004.

[3] L. Tang, L. Cheng, H. Ji and J. Qiu, "Characterization of acoustic black hole effect using a one-dimensional fully-coupled and wavelet-decomposed semi-analytical model," *Journal of Sound and Vibration*, vol. 374, pp. 172–184, 2016.

[4] V.B. Georgiev, J. Cuenca, F. Gautier, L. Simon and V.V. Krylov, "Damping of structural vibrations in beams and elliptical plates using the acoustic black hole effect," *Journal of Sound and Vibration*, vol. 330, no. 11, pp. 2497–2508, 2011.

[5] E.P. Bowyer, D.J. O'Boy, V.V. Krylov and J.L. Horner, "Effect of geometrical and material imperfections on damping flexural vibrations in plates with attached wedges of power law profile," *Applied Acoustics*, vol. 73, pp. 514–523, 2012.

[6] L. Ma and L. Cheng, "Topological optimization of damping layout for minimized sound radiation of an acoustic black hole plate," *Journal of Sound and Vibration*, vol. 458, pp. 349–364, 2019.

[7] M. Ouisse, D. Renault, P. Butaud and E. Sadoulet-Reboul, "Damping control for improvement of acoustic black hole effect," *Journal of Sound and Vibration*, vol. 454, pp. 63–72, 2019.

[8] K. Hook, J. Cheer and S. Daley, "A Parametric Study of an Acoustic Black Hole on a Beam," *The Journal of the Acoustical Society of America*, vol. 145, no. 6, pp. 3488–3498, 2019.

[9] D.J. O'Boy, V.V. Krylov and V. Kralovic, "Damping of flexural vibrations in rectangular plates using the acoustic black hole effect," *Journal of Sound and Vibration*, vol. 329, no. 22, pp. 4672–4688, 2010.

[10] C.A. McCormick, and M.R. Shepherd, "Optimal design and position of an embedded one-dimensional acoustic black hole," in *Proceedings of Inter-Noise 2018*, Chicago, IL, USA, 2018, pp. 26–29.

[11] C.A. McCormick and M.R. Shepherd, "Design optimization and performance comparison of three styles of one-dimensional acoustic black hole vibration absorbers," *Journal of Sound and Vibration*, vol. 420, pp. 1–12, 2020.

[12] V. Denis, A. Pelat, F. Gautier and B. Elie, "Modal overlap factor of a beam with an ABH termination," *Journal of Sound and Vibration*, vol. 333, no. 12, pp. 2475–2488, 2014.

[13] A. Karlos, S. Elliott and J. Cheer, "Higher-order WKB analysis of reflection from tapered elastic wedges," *Journal of Sound and Vibration*, vol. 449, pp. 368–388, 2019.

[14] P.A. Feurtado and S.C. Conlon, "Investigation of boundary-taper reflection for acoustic black hole design," *Journal of Noise Control Engineering*, vol. 5, pp. 460–466, 2015.

[15] J.Y. Lee and W. Jeon, "Vibration damping using a spiral acoustic black hole," *The Journal of the Acoustical Society of America*, vol. 141, no. 3, pp. 1437–1445, 2017.

[16] K. Hook, J. Cheer and S. Daley, "Optimal feedforward control of a beam with an active acoustic black hole termination," in *26th International Congress on Sound and Vibration*, Montreal, Canada, 2019, pp. 1–8.

[17] S. Daley and J. Wang, "A geometric approach to the design of remotely located vibration control systems," *Journal of Sound and Vibration*, vol. 318, pp. 702–714, 2008.

[18] J. Wang and S. Daley, "Broad band controller design for remote vibration using a geometric approach," *Journal of Sound and Vibration*, vol. 329, pp. 3888–3897, 2010.

[19] U. Ubaid, S. Daley, S.A. Pope and I. Zazas, "Design of stable and broadband remote vibration controllers for systems with local nonminimum phase dynamics," *IEEE Transactions on control systems technology*, vol. 24, no. 2, pp. 654–661, 2016.

[20] E. Rustighi, B.R. Mace and N.S. Ferguson, "An adaptive anechoic termination for active vibration control," *Journal of Vibration and Control*, vol. 17, no. 13, pp. 2066–2078, 2011.

[21] C.R. Fuller, S.J. Elliott and P.A. Nelson, *Active Control of Vibration*. London: Academic Press, 1996.

[22] C.R. Halkyard and B.R. Mace, "Feedforward adaptive control of flexural vibration in a beam using wave amplitudes," *Journal of Sound and Vibration*, vol. 254, no. 1, pp. 117–141, 2002.

[23] B.R. Mace and C.R. Halkyard, "Time domain estimation of response and intensity in beams using wave decomposition and reconstruction," *Journal of Sound and Vibration*, vol. 230, no. 3, pp. 561–589, 2000.